Methane Activation at the Pd/CeO$_2$ Interface

Thomas P. Senftle,[†] Adri C. T. van Duin,*[,†,‡] and Michael J. Janik*[,†]

[†]Department of Chemical Engineering, Pennsylvania State University, 140 Fenske Laboratory, University Park, Pennsylvania 16802, United States

[‡]Department Mechanical and Aerospace Engineering, Pennsylvania State University, 240 Research East Building, University Park, Pennsylvania 16802, United States

Ⓢ *Supporting Information*

ABSTRACT: We combine density functional theory (DFT) and reactive force-field (ReaxFF) simulations to assess the stability and activity of unique catalytic sites at the interface between Pd clusters and a CeO$_2$ support. ReaxFF-based Grand Canonical Monte Carlo (GC-MC) simulations provide insight into the oxide structure at the Pd/CeO$_2$ interface. Surface models derived with GC-MC are employed in reactive molecular dynamics (RMD) simulations, which demonstrate that methane lightoff rapidly occurs when there is Pd mixing in the CeO$_2$ lattice. DFT investigations, utilizing models inspired by GC-MC/RMD, demonstrate that Pd^{4+} states are stabilized in PdO$_x$ clusters partially embedded in the CeO$_2$ lattice, and that such sites yield low methane activation barriers. The integrated DFT/ReaxFF methodology employed here demonstrates a combined quantum/classical workflow that can be extended to examine emergent behavior in other oxide-supported metal catalysts.

Pd/CeO$_2$ Catalyst — Pd^{4+} Sites at the Interface

KEYWORDS: *ReaxFF, DFT, methane, palladium, ceria*
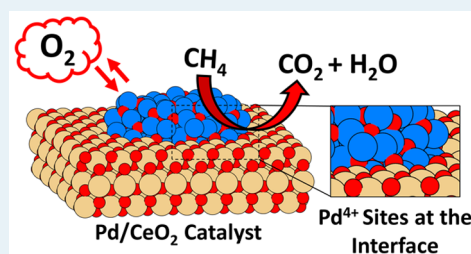
Effective methane conversion—specifically the ability to activate C−H bonds at low temperatures—is essential for the efficient use of abundant natural gas resources and for the abatement of greenhouse gas emissions.[1] Numerous studies point to a synergistic interaction at the Pd/CeO$_2$ interface, leading to rapid catalytic turnover at temperatures lower than those achieved over any other known heterogeneous catalysts. Colussi et al.[2−4] demonstrated that the incorporation of Pd atoms in the CeO$_2$ lattice via solution combustion synthesis yields increased methane oxidation rates, compared to Pd/CeO$_2$ catalysts prepared by incipient wetness impregnation (IWI). Similarly, Cargnello et al.[5] prepared core−shell Pd@CeO$_2$ catalysts that displayed exceptional methane combustion rates, relative to typical IWI analogues. Reports have also demonstrated[6,7] that CO oxidation rates over Pd/CeO$_2$ scale proportionally with the number of sites on the contact line between the Pd cluster and the CeO$_2$ support. Recently, our group demonstrated that there is a tradeoff between stability and activity during methane activation over Pd^{4+} surface states, in which the incorporation of Pd in the CeO$_2$ lattice yields transient and active Pd^{4+} states.[8] This corroborates experimental characterizations by Farrauto et al.[9] and Nilsson et al.,[10] showing that PdO$_x$ formation occurs more readily on CeO$_2$, compared to other supports. Together, these results suggest that CeO$_2$ promotes the oxidation of Pd, which serves as the active phase for catalytic oxidation reactions.

Atomistic details of the active metal/support interfacial site remain elusive, which provides motivation for the use of a combined quantum/classical computational workflow to investigate morphology and activity at the Pd/CeO$_2$ interface (Figure 1). Here, we apply the empirical ReaxFF[11,12] reactive force-field method in tandem with density functional theory (DFT) to assess the formation of mixed Pd−Ce oxide phases. Our results demonstrate that interaction with the CeO$_2$ support stabilizes transient Pd^{4+} states under conditions typical for low-temperature methane combustion. The interaction between Pd and CeO$_2$ thus creates active sites for methane dissociation that emerge from the multicomponent cluster/support interface. The nature of this interaction is closely related to other metal/CeO$_2$ systems in which the incorporation of single metal atoms in the CeO$_2$ lattice is linked to high catalytic activity (e.g., Pt/CeO$_2$[13]).

To model oxide formation in CeO$_2$-supported Pd clusters, we employ a recently developed Grand Canonical Monte Carlo (GC-MC) approach for ReaxFF.[14] This approach builds on a previously developed[15] ReaxFF MC/MD methodology for exploring complex mixed-oxide structures, extending the method to account for a reactive gas-phase environment. Atomistic interactions are described with available Pd/O,[14] Pd/C/H,[16,17] and Ce/O[18] parameter sets. The Pd/O/C/H parameter set is provided in the Supporting Information in ReaxFF input format, and the Ce/O parameter set can be obtained by contacting the corresponding author of ref 18. Additional data regarding the fitting procedure for Pd/Ce/O cross terms developed for this study are provided in the Supporting Information. GC-MC simulations were conducted at varying pressures, where MC moves included the insertion,
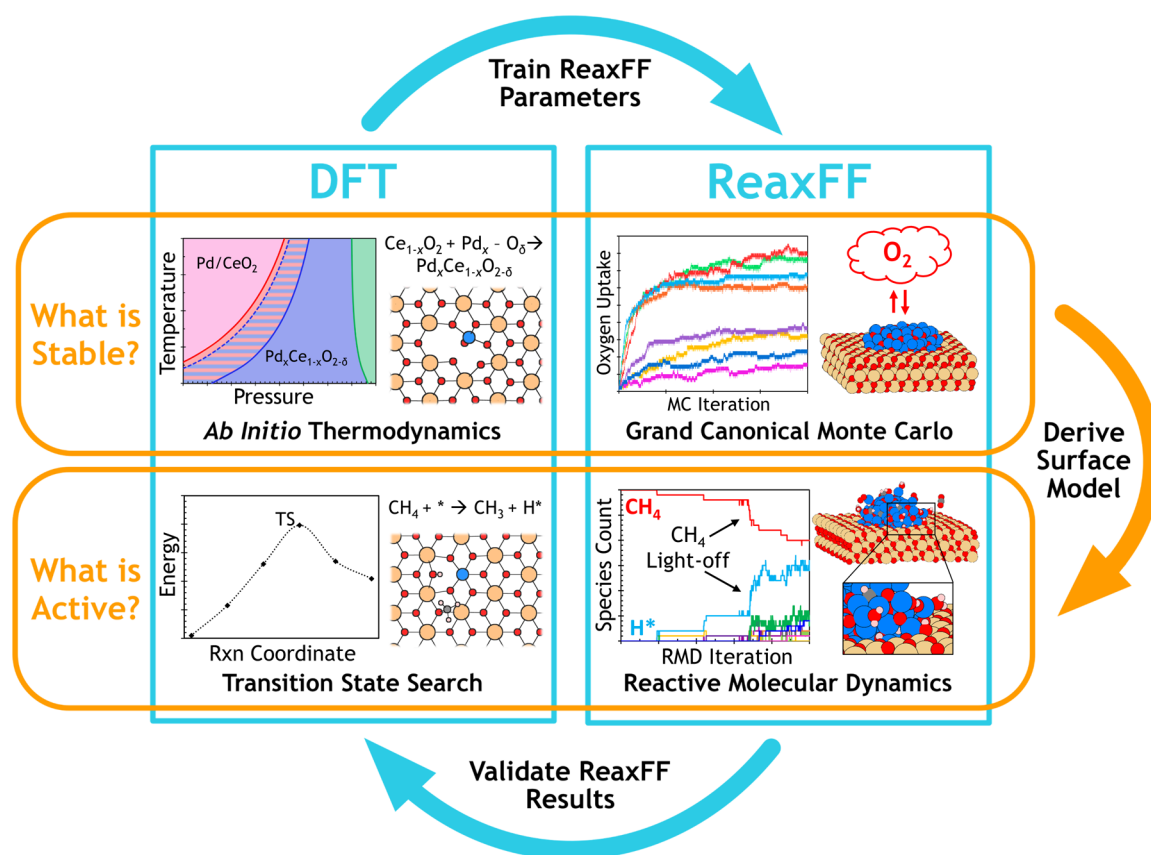
Figure 1. Combined DFT/ReaxFF workflow for investigating the stability and activity of an oxide-supported metal catalyst.

deletion, and translation of O atoms in the Pd cluster on an off-lattice basis (i.e., without predefined insertion sites). The effect of the CeO_2 support on PdO_x formation was assessed using both supported and partially embedded Pd cluster models. The Pd cluster model, motivated by high-resolution transmission electron microscopy (HRTEM) results reported by Cargnello et al.,[6] consists of an ∼15 Å icosahedron cluster that is halved at the center, yielding a (100) surface termination along the basal plane of the cluster. In the supported model, this cluster is placed on a $CeO_2(111)$ surface consisting of three O−Ce−O trilayers in a periodic unit cell with dimensions of 39.8 Å × 33.9 Å × 75.0 Å. In simulations approximating a partially embedded cluster at a roughened Pd/CeO_2 interface, the first O−Ce−O trilayer directly beneath the Pd cluster was removed and the cluster was lowered into the resulting void space. The MC algorithm includes a geometry optimization step at each iteration, allowing the supported and embedded models to structurally relax as the MC run equilibrates (Figure 2a). This is evident in the structures of the supported (Figure 2b) and embedded (Figure 2c) clusters after GC-MC equilibration at a temperature of $T = 500$ K and an oxygen pressure of $P_{O_2} = 1$ atm.

After GC-MC equilibration, there is distinct Pd mixing into the CeO_2 lattice at the edge of the embedded cluster, where Pd atoms migrate toward open lattice positions created by CeO_2 defects (Figure 2c). This behavior is not evident when the Pd cluster is supported on the pristine $CeO_2(111)$ surface (Figure 2b). Additional simulations were conducted at oxygen pressures ranging from 10^{-20} atm to 1 atm at 500 K, which encompass conditions for low-temperature combustion. Higher O:Pd ratios are achieved in embedded Pd clusters at all investigated

pressures (Figure 2a). This corroborates our recent DFT study,[8] which found that oxidized Pd^{4+} states are stabilized by Pd incorporation in the CeO_2 lattice, and this observation supports the experimental findings of Farrauto et al.[9] and Nilsson et al.,[10] demonstrating that CeO_2 enhances PdO_x formation. The simulations reveal that Pd atoms at the cluster/support interface migrate away from the Pd cluster to assume a higher oxygen coordination offered by defect sites in the CeO_2 lattice. Therefore, incorporation will occur readily as Pd atoms and small clusters diffuse across the CeO_2 surface and encounter step, vacancy, or boundary defects.
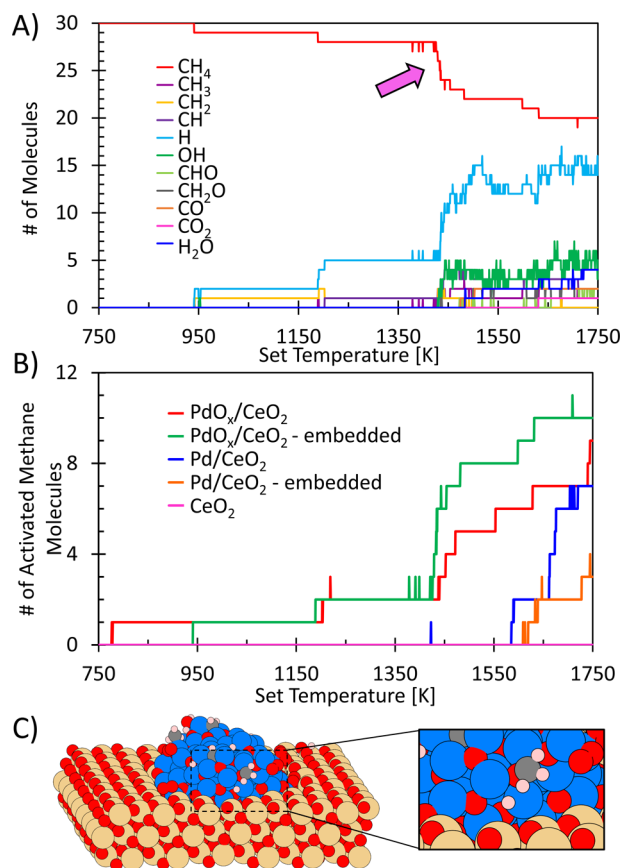
The equilibrated GC-MC structures obtained here serve as surface models for subsequent reactive molecular dynamics (RMD) simulations of methane activation, as they approximate the thermodynamically stable surface morphology under reaction conditions. We employed RMD simulations of methane activation to assess relative activation rates over varying cluster/support interfacial morphologies. A temperature-programmed RMD scheme was used to simulate methane lightoff, where 30 CH_4 molecules were placed randomly in the simulation box above the surface (trajectory videos and coordinates are provided in the Supporting Information). Note that no O_2 molecules are included in the gas phase, as it assumed that the surface has already been equilibrated with the O_2 environment via the GC-MC simulations used to derive the initial geometries. To simulate light-off behavior, the system thermostat was ramped from 750 K to 1750 K over the course of the 50 ps simulation. To monitor methane activation, populations of molecular species were recorded at 25 fs intervals (Figure 3). Methane activation at ∼1440 K is marked by a sharp decrease in the number of gas phase CH_4 molecules
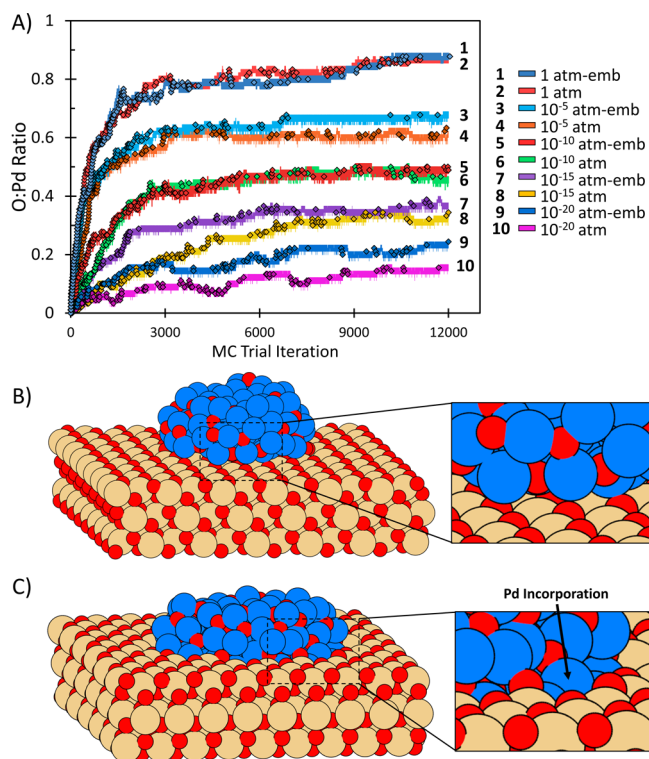
Figure 2. (a) GC-MC simulations of oxygen uptake in supported and embedded Pd clusters on the CeO$_2$(111) surface at 500 K, where denoted pressures correspond to the partial pressure of the oxygen reservoir. Odd- and even-numbered datasets correspond to embedded and supported cluster models, respectively. Lines correspond to MC trial attempts and data points correspond to accepted MC moves. (b, c) Equilibrated structures of the supported PdO$_x$ clusters (panel (b)) and embedded PdO$_x$ clusters (panel (c)) after GC-MC simulation of oxygen uptake at T = 500 K and P_{O_2} = 1 atm.

Figure 3. (a) RMD simulation of methane lightoff over an embedded PdO$_x$ cluster (model derived with GC-MC at T = 500 K and P_{O_2} = 1 atm). (b) Simulated methane light-off curves comparing supported and embedded cluster models. PdO$_x$ models were derived from equilibrated GC-MC simulations at T = 500 K and P_{O_2} = 1 atm, and Pd models were derived from MD simulations equilibrated at T = 500 K in the absence of CH$_4$. (c) RMD snapshot at methane activation lightoff (pink arrow) over the embedded PdO$_x$ cluster model in panel (a).

accompanied by an increase in adsorbed H atoms, indicating dissociative methane adsorption (Figure 3a). Partial combustion products (such as CHO, CH$_2$O, and CO) appear on the surface as intermediate species, along with total combustion products (H$_2$O and CO$_2$) appearing in the gas phase. Figure 3b compares methane lightoff over Pd and PdO$_x$ clusters that are both supported on and embedded in the CeO$_2$ lattice. Control simulations over pristine CeO$_2$(111) resulted in no CH$_4$ activation events. Methane activation occurs more readily over the supported metallic cluster, compared to the embedded cluster, where C−H activation occurs at undercoordinated Pd atoms near the edges of the cluster. Such sites are less accessible to CH$_4$ in the embedded model, leading to slower methane activation. This trend is reversed over the oxidized clusters, where embedded PdO$_x$ achieves faster activation compared to the supported cluster. Since the number of exposed edge sites decreases when the cluster is embedded, enhanced activation over embedded PdO$_x$ must reflect uniquely active sites created by PdO$_x$/CeO$_2$ mixing at the interface (Figure 3c).

The functional form of the ReaxFF potential couples bond order and charge transfer formalisms, which enables the potential to describe covalent, ionic, and mixed covalent/ionic interactions that often occur in supported metal/metal-oxide catalysts. The ability of ReaxFF to describe both covalent and Coulombic interactions makes the potential well-suited for describing the formation of mixed-oxide phases, as has been demonstrated in numerous successful studies that have

employed ReaxFF to investigate multimetal oxides (see, e.g., the work of Chenoweth et al.[15]). The performance of the ReaxFF parameters derived in this work (described in Section 4 in the SI) demonstrate that the potential correctly captures the metastable (and, therefore, reactive) nature of highly oxidized Pd states that form when Pd is mixed into the CeO$_2$ lattice (i.e., Pd incorporation at a Ce lattice site of the fluorite CeO$_2$ structure results in a PdO$_2$ octahedral unit that is reactive because the central Pd is overcoordinated). Increased activity attributed to the Pd/CeO$_2$ interaction is, in this case, adequately described by the bond order formalism of ReaxFF, as the relative stability of PdO and PdO$_2$ units is captured by the energy difference between square planar and octahedral oxygen environments around a Pd center. Although reliable for energetics, ReaxFF is unable to explicitly describe electron transfers, and, for this reason alone, is not sufficient for assessing the electronic nature of metal−support interactions. Therefore, we must use ReaxFF in tandem with electronic structure calculations to unravel concomitant effects at both the electronic and atomistic levels.

To complement the above ReaxFF results, we performed DFT calculations, in conjunction with *ab initio* thermodynamics, to assess the stability and activity of PdO$_x$ formations at

the interface of partially embedded clusters (Figure 4a). DFT calculations were completed with the Vienna *ab initio*
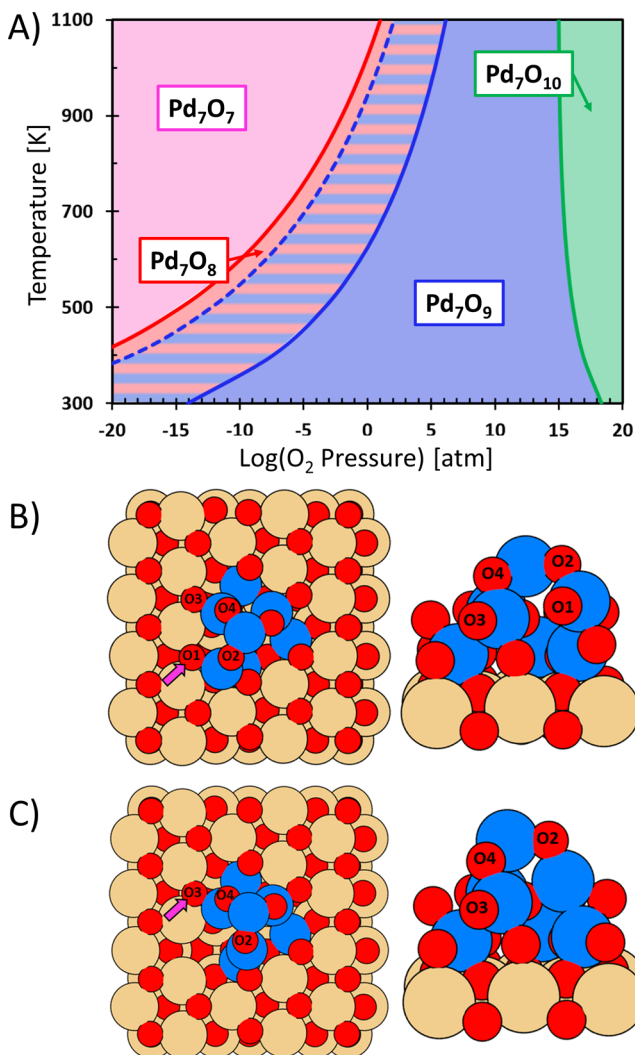
Figure 4. (a) *Ab initio* phase diagram of Pd oxidation states in the $Pd_7O_x/Ce_{33}O_{66}(111)$ model. The solid shaded regions separated by solid lines indicate stable regions in (T,P) space. The striped region and dashed line indicate the region where the supported Pd_7O_8 cluster is thermodynamically stable, yet methane activation is kinetically preferred over the Pd_7O_9 cluster. (b, c) DFT optimized structure of the embedded $Pd_7O_9/Ce_{33}O_{66}(111)$ cluster model (panel (b)) and the $Pd_7O_8/Ce_{33}O_{66}(111)$ cluster model (panel (c)). A cross-sectional view of each model is shown on the right, with the first CeO_2 trilayer omitted for the sake of clarity. Hydrogen abstraction sites during methane activation are indicated by arrows.

simulation package (VASP 5.3.3; computational details are provided in the Supporting Information).[19] Our previous investigation of $Pd_xCe_{1-x}O_\delta$ single-crystal surfaces demonstrated that Pd^{2+} incorporated states are thermodynamically favored under ambient conditions.[8] However, the study also indicated that transient Pd^{4+} states exist during operation, and that such states can offer low methane activation barriers. Here, we extend the $Pd_3Ce_{33}O_{69}(111)$ surface model from that study, which has three Pd^{2+} atoms incorporated in the CeO_2 lattice, to approximate oxide formation in a partially embedded cluster. This is accomplished by placing a Pd_4O_4 cluster in the void space created by oxygen vacancies in the $Pd_3Ce_{33}O_{69}(111)$

surface, thus yielding overall an embedded Pd_7O_7 cluster with exclusively Pd^{2+} oxidation states. Models with Pd^{4+} states are derived by successively adding O atoms on high-symmetry sites of the embedded Pd_7O_7 structure (coordinates of all structures are provided in the Supporting Information). The Pd_7O_8 model was obtained by adding the oxygen atom O2 to the Pd_7O_7 model, and the Pd_7O_9 model was obtained by adding oxygen atom O1 to the Pd_7O_8 model (see Figures 4b and 4c). The optimized PdO_x structures demonstrate a clear tendency for Pd to form square-planar units similar to those found in bulk $P4_2/mmc$ PdO. This suggests that embedding Pd in CeO_2 may aid the formation of small PdO_x clusters, as the reduced fluorite lattice provides square-planar coordination sites for incorporated Pd atoms. This notion is further quantified using *ab initio* thermodynamics to assess the relative stability of supported Pd_7O_x clusters, as a function of temperature and oxygen pressure. The resulting *ab initio* phase diagram demonstrates that partially embedded Pd_7O_x clusters with $x > 7$ (i.e., clusters with Pd^{4+} states) are stable under catalytic combustion conditions (Figure 4a). At 500 K, Pd_7O_x clusters with $x > 7$ are thermodynamically stable at all oxygen pressures above $\sim 10^{-15}$ atm, where the same calculation method demonstrated previously[20] that bulk $P4_2/mnm$ PdO_2 (i.e., all Pd^{4+} states) is less stable than bulk PdO (i.e., all Pd^{2+} states) below oxygen pressures of $\sim 10^{10}$ atm at 500 K. This indicates that CeO_2 enhances oxide formation in embedded Pd clusters, in agreement with the work of Farrauto et al.[9] and Nilsson et al.,[10] allowing Pd^{4+} to be an accessible state under conditions far less oxidizing than what would be required over non-CeO_2 supports.

To assess the activity of sites at the $Pd_7O_x/Ce_{33}O_{66}(111)$ interface, we use a previously validated[8,21,22] pseudo-barrier approach to calculate the apparent free energy of activation via hydrogen abstraction from gas phase CH_4 (this approach is further described in the Supporting Information). The favored hydrogen abstraction site during methane activation over the Pd_7O_8 and Pd_7O_9 surface models, indicated by arrows in Figure 4, resides over O atoms in Ce−O−Pd units at the cluster/support interface. At $T = 500$ K and $P_{O_2} = 0.01$ atm, the Pd_7O_9 surface is less stable than the Pd_7O_8 surface, and therefore, the apparent barrier over the Pd_7O_9 surface consists of the barrier to activate methane summed with the free-energy difference between the Pd_7O_9 and Pd_7O_8 models. This defines a kinetic region in the phase diagram, where the Pd_7O_8 state is thermodynamically stable yet methane activation proceeds through an initial oxidation step, followed by reduction by C−H dissociation. The kinetic region in the figure results from a tradeoff between stability and activity, where a metastable Pd^{4+} state offers a faster activation path, compared to direct activation on the more stable Pd^{2+} state. This analysis is extended to calculate apparent barriers for all $Pd_7O_x/Ce_{33}O_{66}(111)$ models (see Table 1). The apparent barrier and relative rate over the embedded Pd_7O_9 model is commensurate with highly active $Pd_3Ce_{33}O_{69}(111)$[8] and $PdO(101)$[23] surfaces.

To further examine the nature of active sites at the cluster/support interface, we conducted a Bader charge[24,25] analysis of the active sites on the Pd_7O_8 and Pd_7O_9 cluster models (Tables S5 and S6 in the Supporting Information), and we analyzed the distribution of excess spin density after the surface was reduced by the adsorption of a H atom during methane activation (see Figure S3 in the Supporting Information). On the Pd_7O_8

Table 1. Methane Activation Barriers (eV) and Relative Rates[a]

surface site	ΔG_{act} (0 K)	ΔG_{act} (550 K)	ΔG_{form} (550 K)	ΔG_{app} (550 K)	relative rate
$CeO_2(111)$[21]	1.65	2.84		2.84	1
$PdO(101)$[22]	0.50	1.69		1.69	3.4×10^{10}
$Pd_3Ce_{33}O_{72}(111)$[8]	0.43	1.61	2.52	4.13	1.4×10^{-12}
$Pd_3Ce_{33}O_{71}(111)$[8]	0.39	1.57	0.99	2.57	3.1×10^2
$Pd_3Ce_{33}O_{70}(111)$[8]	0.29	1.48	0.31	1.79	4.3×10^9
$Pd_3Ce_{33}O_{69}(111)$[8]	0.68	1.87		1.87	7.7×10^8
$Pd_7O_7/Ce_{33}O_{66}(111)$	1.04	2.23	0.55	2.78	3.6×10^0
$Pd_7O_8/Ce_{33}O_{66}(111)$	1.08	2.27		2.27	1.6×10^5
$Pd_7O_9/Ce_{33}O_{66}(111)$	0.64	1.83	0.01	1.84	1.3×10^9
$Pd_7O_{10}/Ce_{33}O_{66}(111)$	0.52	1.71	0.98	2.69	2.3×10^1

[a]Values calculated using the following parameters: T = 550 K, P_{O_2} = 0.01 atm, and P_{CH_4} = 0.1 atm.

model, both the Bader charge and spin density analyses demonstrate that a Ce^{4+} site at the PdO_x/CeO_2 interface is reduced to Ce^{3+} upon hydrogen abstraction. These analyses reveal on the Pd_7O_9 model that the excess charge from the adsorbed hydrogen atom becomes delocalized across Pd atoms in the PdO_x cluster, and does not localize on an adjacent Ce atom. As such, increased O:Pd ratios stabilized by embedding PdO_x in the CeO_2 lattice lead to highly oxidized Pd atom centers that are readily reduced during methane activation at the interface. Hence, Pd^{2+} is the thermodynamically preferred oxidation state during operation, yet transient Pd^{4+} states can form during the CH_4 activation mechanism. Indeed, reduction of the Pd^{4+} state back to Pd^{2+} drives C−H bond activation, as demonstrated by the charge distribution in Figure S3 in the Supporting Information.

In this work, DFT and ReaxFF were used to assess thermodynamic and kinetic driving forces affecting activity at the Pd/CeO_2 interface. We found that the high methane conversion activity of PdO_x/CeO_2 arises from emergent mixed oxide chemistry at the cluster/support interface. Mixing of Pd into the CeO_2 lattice provides a coordination environment for $Pd^{\delta+}$ species that enable facile alternation between Pd^{2+} and Pd^{4+} oxidation states, thereby creating highly reducible sites ideal for methane activation. The combined use of ReaxFF and DFT allows for a robust study of cluster/support interactions that can elucidate catalyst/support collective behavior at a resolution that cannot be obtained through experiment or isolated computational approaches.

ASSOCIATED CONTENT

Ⓢ Supporting Information

The Supporting Information is available free of charge on the ACS Publications website at DOI: 10.1021/acscatal.6b02447.

> DFT methodology and equations used to generate *ab initio* phase diagrams, coordinates of geometries involved in DFT calculations, description of ReaxFF parameter development, coordinates of equilibrated ReaxFF-GCMC structures, and coordinates/videos of ReaxFF-RMD trajectories (PDF)
> ReaxFF force-field file for Pd/O/C/H (PDF)

AUTHOR INFORMATION

Corresponding Authors
*E-mail: acv13@psu.edu (A. C. T. van Duin).
*E-mail: mjj13@psu.edu (M. J. Janik).

ORCID Ⓞ
Michael J. Janik: 0000-0001-9975-0650

Notes
The authors declare no competing financial interest.

REFERENCES

(1) Farrauto, R. J. *Science* **2012**, 337, 659−660.
(2) Colussi, S.; Gayen, A.; Farnesi Camellone, M.; Boaro, M.; Llorca, J.; Fabris, S.; Trovarelli, A. *Angew. Chem., Int. Ed.* **2009**, 48, 8481−8484.
(3) Colussi, S.; Gayen, A.; Llorca, J.; de Leitenburg, C.; Dolcetti, G.; Trovarelli, A. *Ind. Eng. Chem. Res.* **2012**, 51, 7510−7517.
(4) Colussi, S.; Trovarelli, A.; Cristiani, C.; Lietti, L.; Groppi, G. *Catal. Today* **2012**, 180, 124−130.
(5) Cargnello, M.; Jaén, J. J. D.; Garrido, J. C. H.; Bakhmutsky, K.; Montini, T.; Gámez, J. J. C.; Gorte, R. J.; Fornasiero, P. *Science* **2012**, 337, 713−717.
(6) Cargnello, M.; Doan-Nguyen, V. V. T.; Gordon, T. R.; Diaz, R. E.; Stach, E. A.; Gorte, R. J.; Fornasiero, P.; Murray, C. B. *Science* **2013**, 341, 771−773.
(7) Slavinskaya, E. M.; Kardash, T. Y.; Stonkus, O. A.; Gulyaev, R. V.; Lapin, I. N.; Svetlichnyi, V. A.; Boronin, A. I. *Catal. Sci. Technol.* **2016**, 6, 6650−6666.
(8) Senftle, T. P.; van Duin, A. C. T.; Janik, M. J. *ACS Catal.* **2015**, 5, 6187−6199.
(9) Farrauto, R. J.; Lampert, J. K.; Hobson, M. C.; Waterman, E. M. *Appl. Catal., B* **1995**, 6, 263−270.
(10) Nilsson, J.; Carlsson, P.-A.; Fouladvand, S.; Martin, N. M.; Gustafson, J.; Newton, M. A.; Lundgren, E.; Grönbeck, H.; Skoglundh, M. *ACS Catal.* **2015**, 5, 2481−2489.
(11) van Duin, A. C. T.; Dasgupta, S.; Lorant, F.; Goddard, W. A., III. *J. Phys. Chem. A* **2001**, 105, 9396−9409.
(12) Senftle, T. P.; Hong, S.; Islam, M. M.; Kylasa, S. B.; Zheng, Y.; Shin, Y. K.; Junkermeier, C.; Engel-Herbert, R.; Janik, M. J.; Aktulga, H. M.; Verstraelen, T.; Grama, A.; van Duin, A. C. T. *npj Comput. Mater.* **2016**, 2, 15011.
(13) Pilger, F.; Testino, A.; Carino, A.; Proff, C.; Kambolis, A.; Cervellino, A.; Ludwig, C. *ACS Catal.* **2016**, 6, 3688−3699.
(14) Senftle, T. P.; Meyer, R. J.; Janik, M. J.; van Duin, A. C. T. *J. Chem. Phys.* **2013**, 139, 044109−044115.
(15) Chenoweth, K.; van Duin, A. C. T.; Goddard, W. A. *Angew. Chem., Int. Ed.* **2009**, 48, 7630−7634.
(16) Senftle, T. P.; van Duin, A. C. T.; Janik, M. J. *Catal. Commun.* **2014**, 52, 72−77.

(17) Senftle, T. P.; Janik, M. J.; van Duin, A. C. T. *J. Phys. Chem. C* **2014**, *118*, 4967−4981.

(18) Broqvist, P.; Kullgren, J.; Wolf, M. J.; van Duin, A. C. T.; Hermansson, K. *J. Phys. Chem. C* **2015**, *119*, 13598−13609.

(19) Kresse, G.; Furthmuller, J. *Comput. Mater. Sci.* **1996**, *6*, 15−50.

(20) Mayernick, A. D.; Janik, M. J. *J. Chem. Phys.* **2009**, *131*, 084701−084712.

(21) Krcha, M. D.; Mayernick, A. D.; Janik, M. J. *J. Catal.* **2012**, *293*, 103−115.

(22) Mayernick, A. D.; Janik, M. J. *J. Catal.* **2011**, *278*, 16−25.

(23) Hellman, A.; Resta, A.; Martin, N. M.; Gustafson, J.; Trinchero, A.; Carlsson, P. A.; Balmes, O.; Felici, R.; van Rijn, R.; Frenken, J. W. M.; Andersen, J. N.; Lundgren, E.; Grönbeck, H. *J. Phys. Chem. Lett.* **2012**, *3*, 678−682.

(24) Bader, R. F. W. *Acc. Chem. Res.* **1985**, *18*, 9−15.

(25) Henkelman, G.; Arnaldsson, A.; Jonsson, H. *Comput. Mater. Sci.* **2006**, *36*, 354−360.